Hindawi Publishing Corporation
Advances in Meteorology
Volume 2012, Article ID 505613, 22 pages
doi:10.1155/2012/505613

Research Article

Arctic Climate Variability and Trends from Satellite Observations

Xuanji Wang,[1] Jeffrey Key,[2] Yinghui Liu,[1] Charles Fowler,[3] James Maslanik,[3] and Mark Tschudi[3]

[1] *Cooperative Institute for Meteorological Satellite Studies, University of Wisconsin-Madison, Madison, WI 53706, USA*
[2] *Office of Research and Applications, NOAA/NESDIS, Madison, WI 53706, USA*
[3] *Colorado Center for Astrodynamics Research, University of Colorado at Boulder, Boulder, CO 80309, USA*

Correspondence should be addressed to Xuanji Wang, xuanjiw@ssec.wisc.edu

Received 30 April 2012; Accepted 19 June 2012

Academic Editor: Wansuo Duan

Arctic climate has been changing rapidly since the 1980s. This work shows distinctly different patterns of change in winter, spring, and summer for cloud fraction and surface temperature. Satellite observations over 1982–2004 have shown that the Arctic has warmed up and become cloudier in spring and summer, but cooled down and become less cloudy in winter. The annual mean surface temperature has increased at a rate of 0.34°C per decade. The decadal rates of cloud fraction trends are −3.4%, 2.3%, and 0.5% in winter, spring, and summer, respectively. Correspondingly, annually averaged surface albedo has decreased at a decadal rate of −3.2%. On the annual average, the trend of cloud forcing at the surface is −2.11 W/m^2 per decade, indicating a damping effect on the surface warming by clouds. The decreasing sea ice albedo and surface warming tend to modulate cloud radiative cooling effect in spring and summer. Arctic sea ice has also declined substantially with decadal rates of −8%, −5%, and −15% in sea ice extent, thickness, and volume, respectively. Significant correlations between surface temperature anomalies and climate indices, especially the Arctic Oscillation (AO) index, exist over some areas, implying linkages between global climate change and Arctic climate change.

1. Introduction

Recent observations have shown dramatic decreases in Northern Hemisphere sea ice extent and thickness [1–9]. Over the last two decades, the changes in many aspects of the Arctic climate system have been observed, including surface temperature and albedo, atmospheric circulation, precipitation, snowfall, biogeochemical cycle, and vegetation [10–16]. Arctic climate change is also reflected in the changes in climate indices such as the Arctic Oscillation (AO), which indicates that a significant change in the climate system occurred in the late 1970s and early 1980s [17–21]. How the interactions and feedbacks of all climate components play a role in Arctic climate change is a challenging issue. A recent study, for example, shows how clouds respond to changes in sea ice cover, such that a cloudier Arctic is expected with less sea ice cover in the future [22]. Numerous climate modeling studies have shown that the Arctic is one of the most sensitive regions to global climate change as a result of the positive feedback between surface temperature, surface albedo, and ice extent, known as the ice-albedo feedback [23–27]. This fundamental theory has been confirmed by a variety of observational evidence, though records of Arctic climate change are relatively brief and, for surface observations, geographically sparse.

This paper summarizes recent Arctic climate variations and trends in surface, sea ice, cloud, and radiation properties over the period of 1982–2004. Satellite data form the basis of the analyses, in particular the extended Advanced Very-High-Resolution Radiometer (AVHRR) Polar Pathfinder (APP-x) satellite data set. Possible linkages with the low-latitude climate change will also be discussed. The paper extends our previous work [13–15] with a longer times series (extended from 18 to 23 years), the introduction of ice properties, and improved satellite retrieval algorithms. Major changes to the satellite retrieval algorithms include the addition of polar stratospheric cloud (PSC) detection and cloud type labeling, revised look-up tables for retrieving cloud optical depth, particle size, and particle phase, improved cloud mask detection, and more accurate surface temperature and albedo retrievals.

2. Data Sets and Analysis Approach

The primary data set used here is a multiparameter product suite called the extended AVHRR Polar Pathfinder (APP-x) [28–30]. The APP-x data products include cloud fraction, cloud optical depth, cloud particle phase and size, cloud top pressure and temperature, surface skin temperature, surface broadband albedo, sea ice thickness, radiative fluxes, and cloud radiative effects ("cloud forcing"). The product retrievals were done with the Cloud and Surface Parameter Retrieval (CASPR) system [31–35]. APP-x consists of twice daily composites at a $25 \times 25\,\text{km}^2$ pixel size for the Arctic and Antarctica, currently over the period 1982–2004, though it is being extended in time to the present at a spatial resolution of 5 km. The spatial coverage for the Arctic is shown in Figure 1. APP-x is consistent over time with no observable bias [13]. Validation was done mainly with the data collected during the Surface Heat Balance of the Arctic Ocean (SHEBA) field experiment in the western Arctic [36–38] and with data from two Antarctic meteorological stations: South Pole and Neumayer [39]. The uncertainties of the APP-x data products were discussed and presented by Wang and Key [14].

The secondary data set used in this study is sea ice concentration derived from Nimbus-7 Scanning Multi-channel Microwave Radiometer (SMMR) and Defense Meteorological Satellite Program (DMSP) -F8, -F11, and -F13 Special Sensor Microwave/Imager (SSM/I) radiances at a grid cell size of $25 \times 25\,\text{km}^2$ using the NASA Team Algorithm [41], available from the National Snow and Ice Data Center (NSIDC) at http://nsidc.org/data/nsidc-0051.html. The sea ice concentration data were used to identify sea ice and to estimate sea ice extent and sea ice age over the study period.

Commonly used climate index data are from a variety of data sources. The Arctic Oscillation (AO), North Atlantic Oscillation (NAO), Antarctic Oscillation (AAO), and Pacific/North American Pattern (PNA) indices are from the NOAA/Climate Prediction Center (CPC). The Pacific Decadal Oscillation (PDO) index is from the Joint Institute for the Study of the Atmosphere and Ocean (JISAO). The Multivariate ENSO Index (MEI) is from NOAA Earth System Research Laboratory. The Oceanic Nino Index (ONI) is from NOAA/NWS/CPC, and the Southern Oscillation Index (SOI) is from NCAR/CGD's Climate Analysis Section.

In addition to basic analyses of the variations of climate parameters for the Arctic, trend analyses of the seasonal and interannual variability of surface, sea ice, cloud properties, and radiation components were performed using least-squares regression with the 23-year APP-x products over the period 1982–2004. The trend analysis method was described in detail in the paper by Wang and Key [15]. Unless noted otherwise, all trends reported here are statistically significant at the confidence level of 90% or higher. Each of the Arctic climate parameters was regressed with the year as the independent variable, and the trend value is the slope of the linear regression line along with a standard deviation (SD) of the slope.

The analyses were done for the entire Arctic region north of 60°N and its 18 subregions. The trends were calculated for the 18 climate variables listed in Table 1. Table 2 gives the annual trends of the 18 climate parameters for some Arctic areas. The trends will be discussed in more detail in the following sections. The 18 subregions are shown in Figure 1, where the subregions or areas are named and indicated by the numbers in the parentheses. Definitions of these subregions follow Thomas and Rothrock (1993) [42] and Groves and Francis (2002) [12] to be consistent with those defined in the studies of the Arctic Ocean freshwater budget. Land region subdivisions are based on the geographic naming convention. Two other Arctic Ocean divisions were also used for the larger ocean regions. One follows Groves and Francis [43] that includes a Pacific sector (regions 1–4), Eastern/Central (region 5–7), Arctic basin (regions 1–7), and Atlantic sector (regions 8-9) and GIN Seas (region 9). The other is from Serreze and Barry [44], which divided the Arctic Ocean into three larger regions that are Central Arctic Ocean, Arctic Ocean, and Polar Cap (poleward of 70°N), as shown in Figure 2. The Arctic landmasses north of 60°N were divided into the six subregions in Figure 1: North Europe (region 13), North Central Russia (region 14), Northeastern Russia (region 15), Alaska Region (region 16), North Canada (region 17), and Greenland (region 18).

Table 1: Symbols and physical meanings of the 18 retrieved climate parameters.

PID name	Physical meaning
T_s	Surface temperature (°C or K).
α_s	Broadband albedo (range: [0, 1]).
Re	Cloud droplet effective radius (μm).
τ_c	Cloud optical depth (unitless).
ϕ_c	Cloud particle phase (0 = liquid, 100 = ice).
T_c	Cloud top temperature (°C or K).
P_c	Cloud top pressure (hPa).
PW	Precipitable water (cm).
$\text{SW}\downarrow_{\text{srf}}$	Downwelling shortwave radiation at the surface (W/m^2).
$\text{LW}\downarrow_{\text{srf}}$	Downwelling longwave radiation at the surface (W/m^2).
$\text{SW}\uparrow_{\text{srf}}$	Upwelling shortwave radiation at the surface (W/m^2).
$\text{LW}\uparrow_{\text{srf}}$	Upwelling longwave radiation at the surface (W/m^2).
$\text{SW}\downarrow_{\text{toa}}$	Downwelling shortwave radiation at the TOA (W/m^2).
$\text{SW}\uparrow_{\text{toa}}$	Upwelling shortwave radiation at the TOA (W/m^2).
$\text{LW}\uparrow_{\text{toa}}$	Upwelling longwave radiation at the TOA (W/m^2).
CF_S	Shortwave cloud forcing at the surface (W/m^2).
CF_L	Longwave cloud forcing at the surface (W/m^2).
A_c	Cloud fraction (0–100, unitless).

3. Surface

Surface temperature and albedo are two critical factors of the climate system, reflecting the dominant state of the climate system. Results for these two parameters are shown in Figure 3. The time series and their trends in surface skin temperature and broadband albedo over 1982–2004 were calculated for each $25 \times 25\,\text{km}^2$ resolution pixel over

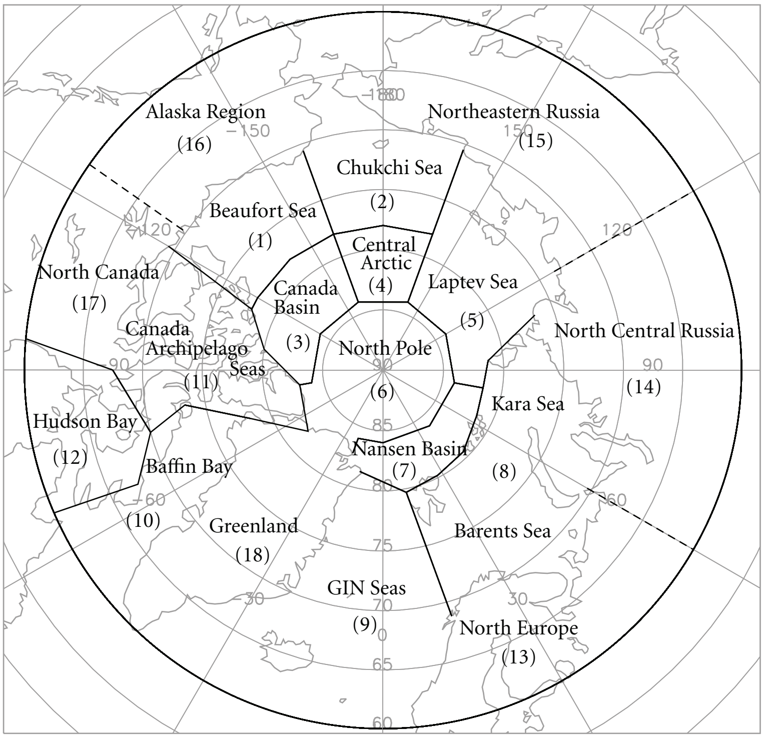

Figure 1: Regional divisions of the Arctic region north of 60°N.

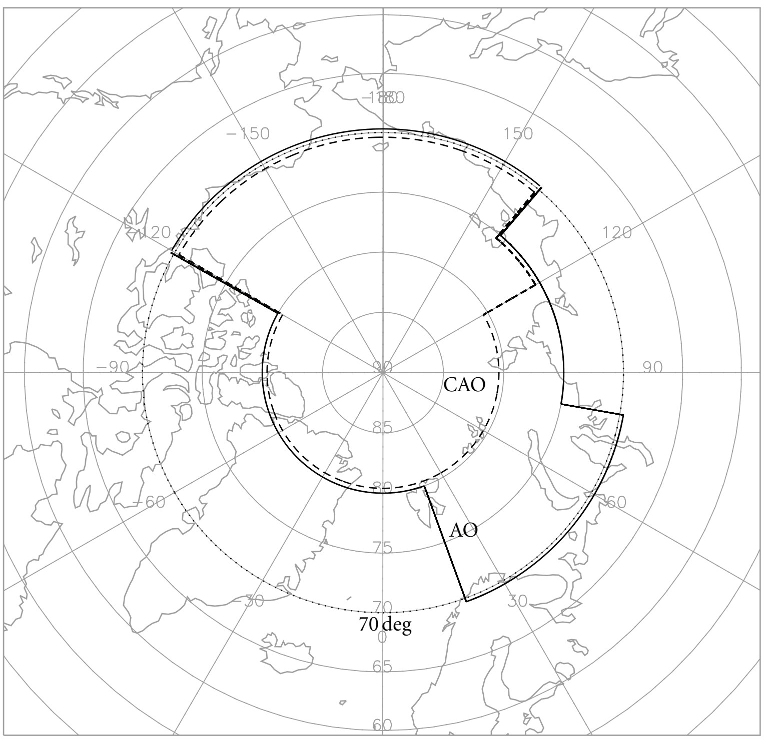

Figure 2: Regional divisions of the Arctic Ocean north of 70°N from Serreze et al. [40]: Central Arctic Ocean (CAO, dashed), Arctic Ocean (AO, solid), and Polar Cap (70°N, dotted).

Table 2: Parameter means, standard deviations, and confidence levels by region.

Parameter and units	Region: Arctic region north of 60°N	Arctic ocean north of 60°N	Arctic land north of 60°N	Greenland island	Polar cap north of 70°N	Arctic ocean (AO)	Central arctic ocean (CAO)
T_s (°C)	0.0339 ± 0.0156 (96%)	0.0052 ± 0.01366 (30%)	0.0636 ± 0.0210 (99%)	0.0718 ± 0.0324 (96%)	−0.0069 ± 0.0162 (32%)	−0.0661 ± 0.0273 (98%)	0.0116 ± 0.0195 (44%)
α_s (0 to 1)	−0.0025 ± 0.0007 (99%)	−0.0026 ± 0.0008 (99%)	−0.0025 ± 0.0007 (99%)	−0.0035 ± 0.001 (99%)	−0.0029 ± 0.0009 (99%)	−0.001 ± 0.001 (69%)	−0.003 ± 0.001 (99%)
Re (μm)	0.0504 ± 0.0799 (47%)	0.0373 ± 0.0835 (34%)	0.0640 ± 0.0771 (58%)	0.0446 ± 0.0927 (37%)	0.0560 ± 0.0846 (48%)	0.0478 ± 0.0803 (44%)	−0.0031 ± 0.0853 (3%)
τ_c (unitless)	−0.0018 ± 0.0016 (70%)	−0.0038 ± 0.0014 (99%)	0.0003 ± 0.0022 (11%)	0.0019 ± 0.0043 (34%)	−0.0036 ± 0.0016 (97%)	−0.0050 ± 0.0016 (99%)	0.0012 ± 0.0028 (32%)
ϕ_c (0 = liquid, 100 = ice)	0.1880 ± 0.1019 (92%)	−0.1992 ± 0.1669 (90%)	0.1763 ± 0.0901 (94%)	0.2151 ± 0.0941 (97%)	0.3197 ± 0.1245 (98%)	0.1462 ± 0.1243 (75%)	0.3334 ± 0.1378 (98%)
T_c (°C)	0.0068 ± 0.0132 (39%)	0.0139 ± 0.0143 (66%)	0.0007 ± 0.0136 (4%)	0.0055 ± 0.0264 (16%)	0.0181 ± 0.0160 (73%)	−0.0390 ± 0.0181 (96%)	0.0426 ± 0.0168 (98%)
P_c (hPa)	−0.5080 ± 0.1820 (99%)	−0.5619 ± 0.1836 (99%)	−0.4520 ± 0.1925 (97%)	−0.6006 ± 0.3069 (94%)	−0.5164 ± 0.2126 (98%)	−0.7547 ± 0.2722 (99%)	−0.1226 ± 0.2604 (36%)
PW (cm)	0.0015 ± 0.0006 (99%)	0.0020 ± 0.0006 (99%)	0.0010 ± 0.0006 (87%)	0.0014 ± 0.0005 (99%)	0.0016 ± 0.0006 (99%)	0.0007 ± 0.0011 (51%)	0.0024 ± 0.0008 (99%)
$SW\downarrow_{srf}$ (W/m^2)	−0.1028 ± 0.0958 (71%)	−0.0376 ± 0.805 (35%)	−0.1705 ± 0.1549 (72%)	0.0725 ± 0.4205 (1%)	−0.1375 ± 0.0915 (85%)	−0.1047 ± 0.1358 (55%)	−0.1520 ± 0.1411 (71%)
$LW\downarrow_{srf}$ (W/m^2)	0.1231 ± 0.0639 (93%)	−0.0040 ± 0.0646 (5%)	0.2548 ± 0.0738 (99%)	0.1122 ± 0.1743 (47%)	−0.0726 ± 0.0768 (65%)	−0.1525 ± 0.1116 (81%)	−0.0350 ± 0.1022 (26%)
$SW\uparrow_{srf}$ (W/m^2)	−0.4095 ± 0.1044 (99%)	−0.4321 ± 0.1214 (99%)	−0.3861 ± 0.1376 (99%)	−0.4959 ± 0.3391 (84%)	−0.4533 ± 0.1302 (99%)	−0.1693 ± 0.1797 (64%)	−0.5243 ± 0.1858 (99%)
$LW\uparrow_{srf}$ (W/m^2)	0.1571 ± 0.0644 (98%)	0.0311 ± 0.0571 (41%)	0.2878 ± 0.0830 (99%)	0.2259 ± 0.1133 (94%)	−0.0209 ± 0.0653 (25%)	−0.2589 ± 0.1212 (96%)	0.0476 ± 0.0767 (46%)
$SW\downarrow_{toa}$ (W/m^2)	0.0157 ± 0.0851 (15%)	0.027 ± 0.0576 (4%)	0.0294 ± 0.1157 (20%)	−0.0159 ± 0.386 (31%)	−0.0285 ± 0.0323 (61%)	−0.0342 ± 0.0394 (61%)	−0.0298 ± 0.0321 (64%)
$SW\uparrow_{toa}$ (W/m^2)	−0.3366 ± 0.1879 (91%)	−0.4321 ± 0.1822 (97%)	−0.2376 ± 0.1992 (75%)	−0.5896 ± 0.2643 (96%)	−0.3867 ± 0.1577 (98%)	−0.1229 ± 0.2140 (43%)	−0.4617 ± 0.1765 (98%)
$LW\uparrow_{toa}$ (W/m^2)	0.0260 ± 0.0214 (76%)	0.0227 ± 0.0215 (70%)	0.0294 ± 0.0266 (72%)	0.0776 ± 0.0416 (92%)	0.0170 ± 0.0257 (48%)	−0.1012 ± 0.0420 (98%)	0.0306 ± 0.0348 (61%)
CF_S (W/m^2)	−0.1790 ± 0.0634 (99%)	−0.0604 ± 0.0630 (65%)	−0.3019 ± 0.0854 (99%)	−0.1166 ± 0.0918 (78%)	−0.1484 ± 0.0618 (97%)	−0.0282 ± 0.1288 (17%)	−0.1940 ± 0.0851 (97%)
CF_L (W/m^2)	−0.0318 ± 0.0308 (68%)	−0.0797 ± 0.0371 (96%)	0.0177 ± 0.0300 (3%)	−0.0816 ± 0.1156 (51%)	−0.1023 ± 0.0418 (98%)	−0.0242 ± 0.0403 (45%)	−0.1195 ± 0.0637 (93%)
A_c (0 to 100)	−0.0242 ± 0.0505 (36%)	−0.0898 ± 0.0580 (86%)	0.0438 ± 0.0473 (64%)	−0.2013 ± 0.1369 (85%)	−0.1588 ± 0.0653 (98%)	0.0622 ± 0.0647 (65%)	−0.2636 ± 0.1011 (98%)

The number in parenthesis is the F test confidence level for the trend.

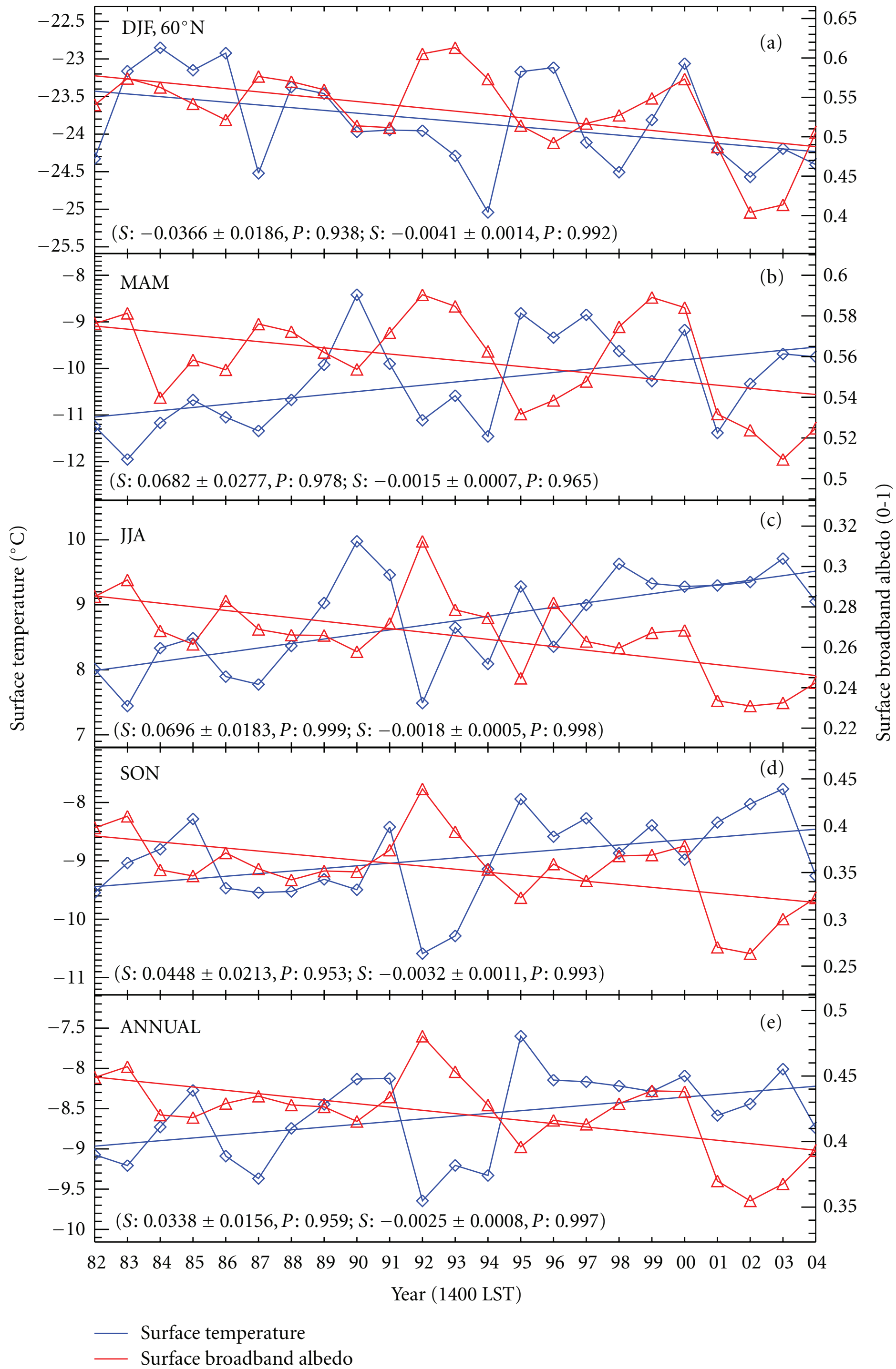

FIGURE 3: Time series and trends of surface skin temperature and broadband albedo in winter (DJF), spring (MAM), summer (JJA) and Autumn (SON) over the period of 1982 to 2004 for the Arctic region north of 60°N. Numbers in parentheses are the trend slope per year ("S") with its standard deviation and the F test confidence level ("P"). The first pair of S and P denotes the surface temperature trend (blue) and the second pair is for the surface albedo (red).

the entire Arctic region north of 60°N for winter (December–February, where December data are from the previous year, marked as DJF in the upper-left corner of the Figure 3), spring (March—May, marked as MAM), summer (June—August, marked as JJA), autumn (September—November, marked as SON), and for the annual mean (marked as ANNUAL).

Overall, the Arctic surface temperature has decreased significantly at the annual rate of −0.037°C in winter with an SD of 0.019°C. Major cooling has occurred around

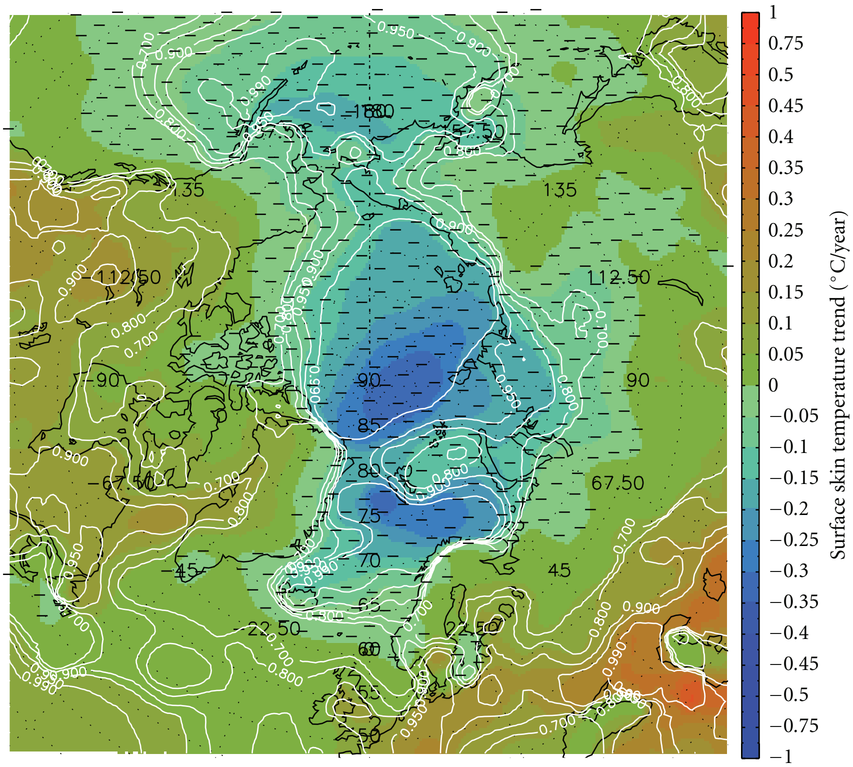

Figure 4: Surface skin temperature trend image for the Arctic in winter over the period of 1982 to 2004. The contours in the image indicate the confidence levels, and color represents the surface temperature trend in degrees per year. Areas with cooling trends are marked with dashes.

the central and eastern Arctic Ocean as shown in Figure 4. This finding is consistent with the work by Serreze et al. [40], which showed a cooling trend in the northern North Atlantic. For the Polar Cap, which is the area north of 70°N, the surface temperature has decreased by −0.125°C per year with an SD of 0.042°C. In the meantime, the wintertime surface broadband albedo has actually decreased at the annual rate of −0.41% with an SD of 0.14%. The reason is that a large part of the Arctic region is dark throughout winter; the albedo trend only represents areas between 60°N and approximately 76°N.

While during the warm seasons from spring to autumn, the surface temperature has increased at the annual rates of 0.068°C, 0.070°C, and 0.045°C with the SDs of 0.028°C, 0.018°C, and 0.021°C, respectively. Correspondingly, the surface albedo has decreased at the annual rate of −0.32% with an SD of 0.11% in autumn, indicating later freeze-up and snowfall [45]. Figure 5 shows the spatial distribution of the surface albedo trends in autumn, indicating large negative trends over the central and eastern Arctic Ocean, Beaufort and Chukchi Seas. This agrees with the trends in sea ice concentration, thickness, and snow cover reported by other researchers [46–51].

On the annual average over the entire Arctic region, the annual mean trend in surface temperature shows warming at the annual rate of 0.034°C with an SD of 0.016°C. This warming comes primarily from the significant warming in spring and summer. Correspondingly, the annual mean surface albedo has decreased at the annual rate of −0.25% with an SD of 0.08%.

4. Cloud

Clouds are indicators of atmospheric stability, humidity, and circulation. Clouds interact with other climate parameters, such as surface temperature and the radiation field, to manipulate or mitigate climate change through complex feedback mechanisms [51, 52]. A better understanding of the changes in cloud and its interactions with other parameters will benefit the understanding the complex Arctic climate system. Figures 6–9 show the time series and trends in cloud properties including fraction, particle effective radius, optical depth, particle phase, top temperature, and top pressure along with atmospheric precipitable water for the four seasons and the annual mean over the entire Arctic region.

In winter, Arctic cloud cover fraction has decreased at the annual rate of −0.34% with an SD of 0.14% (Figure 6). Over the central Arctic, cloudiness has actually begun declining in late autumn at the annual rate of about −0.50% and continued and increased in magnitude into winter. Wang and Key [14] argued that the decrease in cloud cover over the Arctic Ocean is associated with reduced moisture convergence over the Nansen Basin and parts of the Barents and

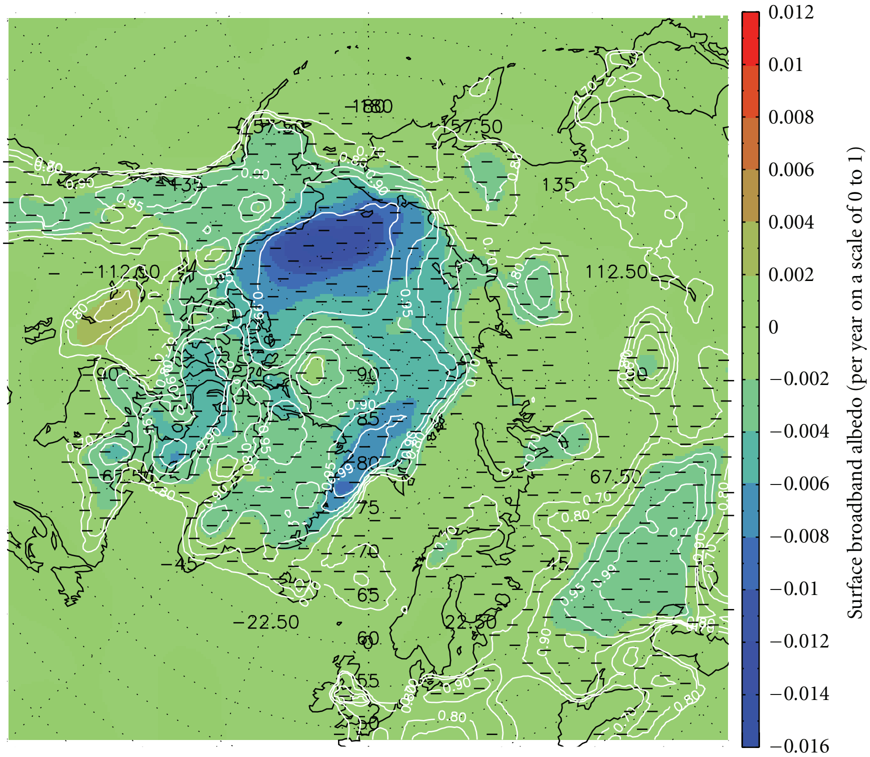

Figure 5: As in Figure 4, but for the surface albedo trend in autumn (September, October, and November, SON). Areas with decreasing trends are marked with dashes.

Kara Seas due to weakening cyclonic activity and subsequent advection of that somewhat drier air mass to the east. The reduced warming effect of the decreasing cloud cover over the Arctic Ocean in the winter contributes to the cooling trend in the surface temperature [51].

Some other cloud bulk microphysical and optical characteristics have also changed. Figure 8 shows the time series and trends of cloud particle effective radius, optical depth, and particle phase. Cloud particle phase is indicated by two numbers: 0 for liquid phase, 100 for solid phase (ice), and a number between 0 and 100 stands for averages over time and/or space. A number less than 50 indicates that liquid-phase clouds dominate; a value greater than 50 indicates that ice clouds dominate. The cloud particle effective radius for liquid droplets is the ratio of the third to second moments of the drop size distribution as defined by Wang and Key [14]. Ice crystal optical properties are based on the parameterization of Key et al. [33]. The cloud particle phase shows positive trend in winter indicating ice cloud increase. Overall for the Arctic, cloud particle effective radius and optical depth show no trends, though some of the specific areas have trends such as the North Pole where there is an increasing trend in cloud particle effective radius at the annual rate of 0.5 μm with an SD of 0.1 μm in correspondence to the increasing cloud particle phase trend there. The cloud top temperature has increased in the western Arctic Ocean and North Canada, but decreased in the north eastern and north central Russia. The spatial distribution pattern of the cloud top temperature trends is similar to that of the surface temperature trend, that is, warming in the east and cooling in the west. For most of the Arctic areas, there are positive trends in cloud top height (decreasing cloud top pressure), while there are a few instances of negative trends in cloud height (increasing cloud top pressure) in the Canada Basin and Central Arctic.

In warm seasons including spring, summer, and autumn, the only significant cloud fraction trend is in spring that has increased at the annual rates of 0.23% with an SD of 0.06%. The increasing cloudiness in spring has occurred primarily in the Arctic Ocean area north of 70°N, that is, the Polar Cap, at the average annual rate of 0.47% with an SD of 0.12% (Figure 7). In summer a small increase of the cloud fraction was in large part observed over the Canada Basin and North Central Russia where the annual rate of the cloud fraction increase is about 0.25%. Most of the other areas do not exhibit trends. In spring, there are no statistically significant trends found in cloud particle effective radius, cloud optical depth, or cloud particle phase for the entire Arctic region, though both cloud optical depth and particle phase show some declines. There are also no significant trends in cloud optical depth and cloud particle effective radius found in summer or autumn, except that the clouds have been increasing in liquid phase in summer. There is a small negative trend in effective radius in summer over the western Arctic Ocean and a positive trend in liquid-phase clouds in the GIN Seas and Barents Sea. The effective radius

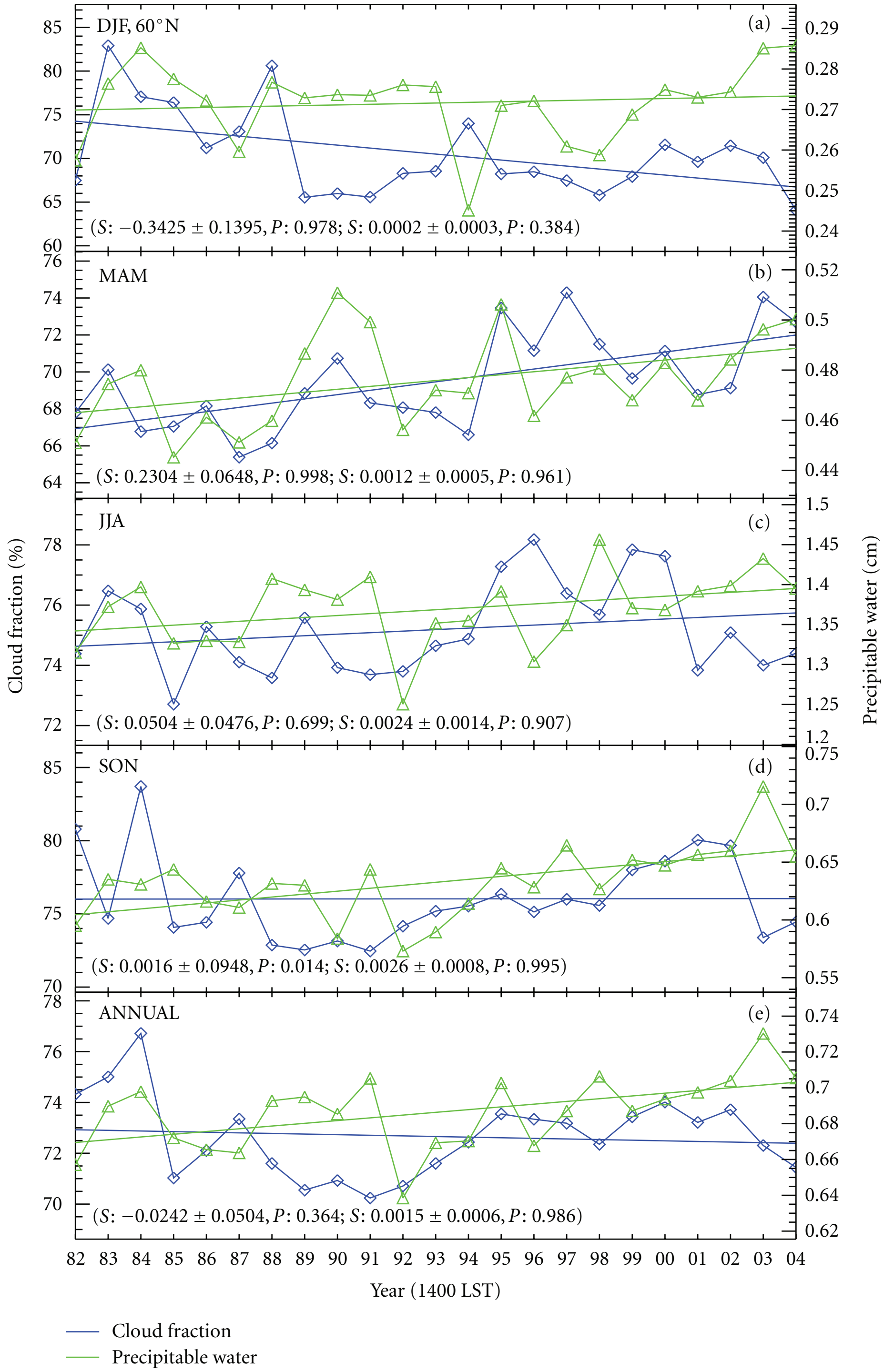

Figure 6: As in Figure 3 but for cloud fraction and precipitable water. The first pair of S and P denotes the cloud fraction trend (blue) and the second pair is for the precipitable water trend (green).

has a negative trend, though not statistically significant, in autumn at the annual rate of about $-0.10\,\mu$m with the significant trends found in the Chukchi Sea, Beaufort Sea, Canada Archipelago Seas, Canada Basin, and the eastern part of Greenland. Overall, in autumn cloud particle phase does show a positive trend in the Arctic, with most of the contribution from the central and eastern Arctic Ocean areas. The cloud top temperature does not exhibit any statistically significant trends persistently over all four seasons, except in spring the cloud top temperature shows increases in the west Arctic and decreases in the east Arctic, primarily in North Europe. In contrast, there are significant negative trends

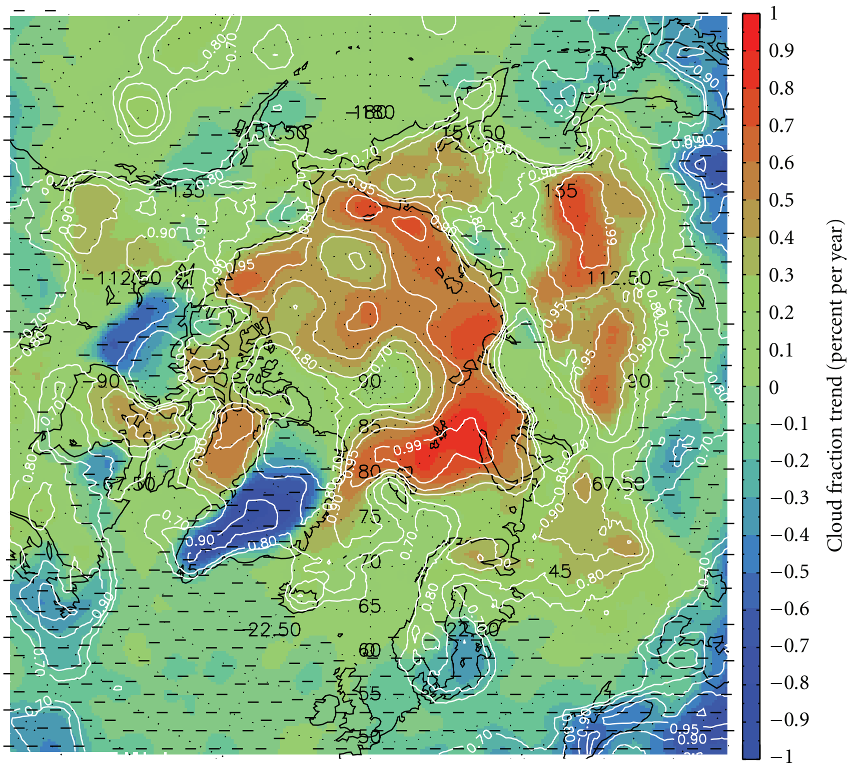

Figure 7: As in Figure 4, but for the cloud fraction in spring (March, April, and May, MAM). Areas with decreasing trends are marked with dashes.

found in cloud top pressure in spring, summer, autumn, and annual mean, indicating the cloud top height getting higher with time in the warmer seasons.

On an annual time scale, the seasonal trends cancel, resulting in no cloud fraction trend overall for the entire Arctic region, with most of the Arctic Ocean areas having declining trends in cloudiness due to the strong winter negative trends in those ocean areas. The cloud particle phase has an increasing rate of 0.19 per year with an SD of 0.10, mainly over the Arctic land areas. The cloud particle effective radius and optical depth exhibit no significant trends at all. The cloud top temperature has no trend at all for the entire Arctic region, while cloud top pressure does show a positive trend. Given that cloud top temperature is estimated from the satellite data but cloud top pressure is obtained from the model temperature profile based on the retrieved temperature, this apparent inconsistency in the trends of the two parameters probably implies a change in atmospheric structure.

The positive trends in most of the cloud properties in the warm seasons are generally consistent with an increasing trend in cyclonic activity [40] and an increasing trend in total precipitable water (PW) obtained directly from the independent NCEP/NCAR Reanalysis data set. Over the Arctic Ocean north of 60°N, there is almost no trend in PW during winter due to the cold and dry air, while during spring, summer, and autumn the PW has been increasing at the annual rates of 0.0012 cm, 0.0024 cm, and 0.0026 cm with the SDs of 0.0005, 0.0014, and 0.0008 cm, respectively, as shown in Figure 6. This is consistent with surface temperature trends and supports the satellite retrievals, at least qualitatively. Overall, the annual mean PW trend is 0.0020 cm per year with an SD of 0.0006 cm over the Arctic Ocean. For the landmasses north of 60°N, there are significant trends in PW found for some areas, for example, Greenland, which has an increasing annual rate of 0.0014 cm with an SD of 0.0005 cm, most of which is from autumn with the rate of 0.0029 cm per year and an SD of 0.006 cm).

5. Radiation

The surface radiative field controls the surface energy budget that determines the surface temperature, impacts sensible and latent heat capacities and boundary layer dynamic conditions. In that Arctic, the ice/snow-albedo feedback plays a key role in balancing the surface energy budget. As surface temperature increases, the ice/snow thickness and extent are expected to decrease, which in turn leads to decrease in surface albedo and increase in the absorbed shortwave radiative flux at the surface. Understanding the surface radiation field change is very helpful to better understand the cloud radiative effect, that is, so-called "cloud forcing" which is defined as the difference between net all-sky radiative flux and net clear-sky radiative flux. Therefore a positive cloud forcing indicates a warming effect and a negative value indicates a cooling effect on the surface or at the top of the atmosphere (TOA) incurred by clouds.

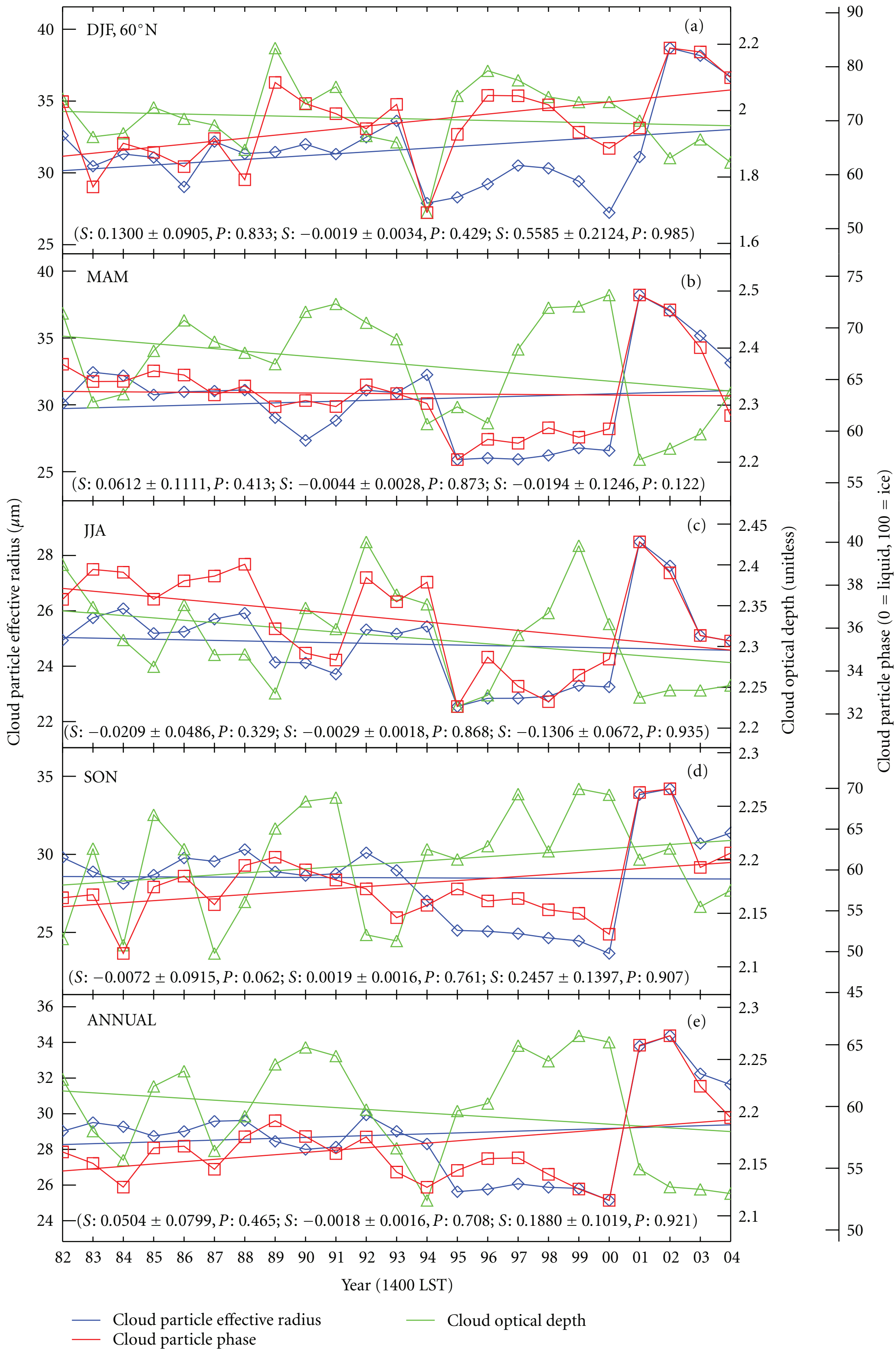

FIGURE 8: As in Figure 3, but for cloud particle phase, effective radius and optical depth. The first pair of S and P denotes the cloud particle effective radius trend (blue), the second pair is for the cloud optical depth trend (green), and the third pair represents the cloud particle phase trend (red).

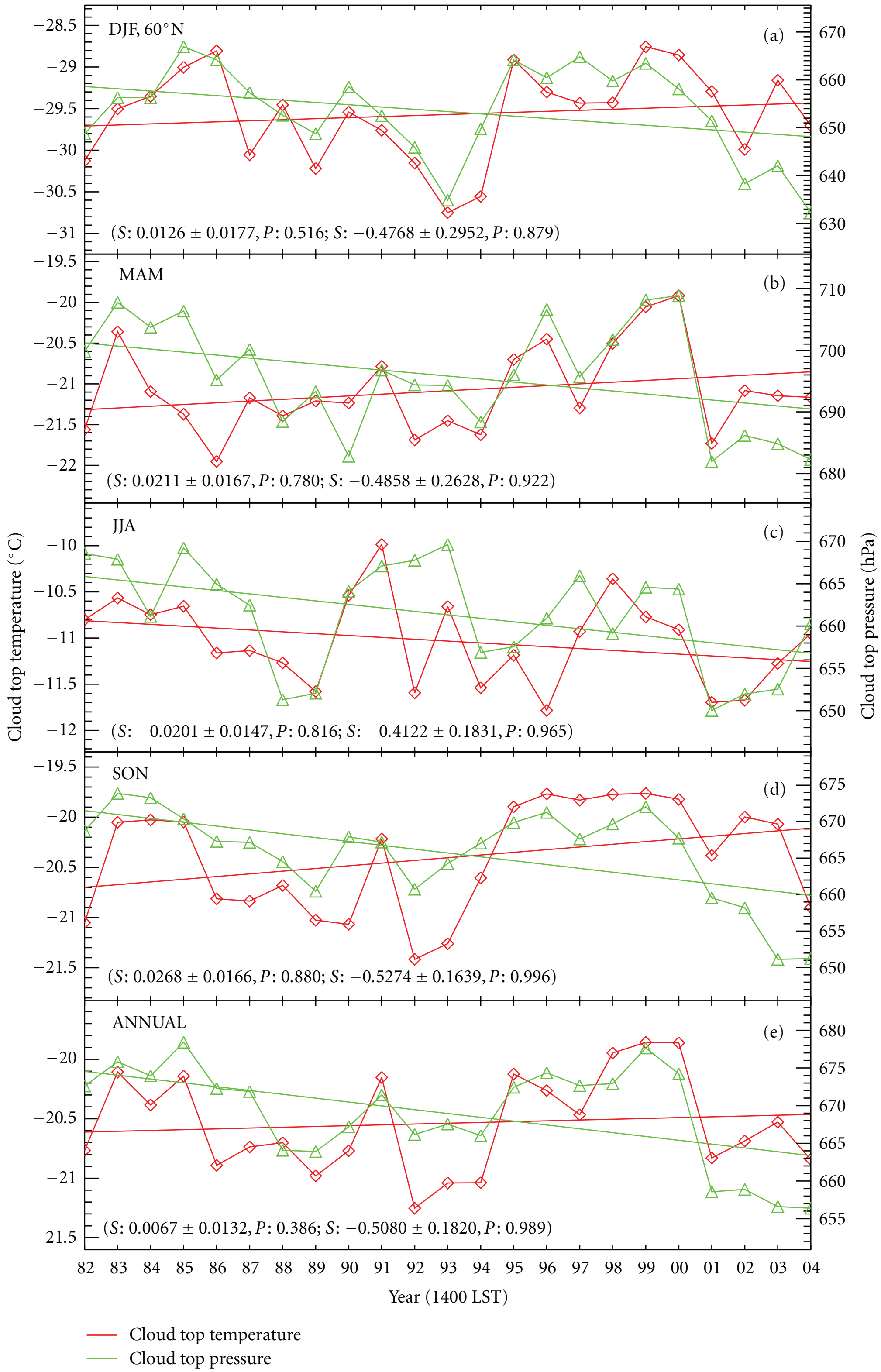

FIGURE 9: As in Figure 3, but for cloud top temperature and pressure. The first pair of S and P denotes the cloud top temperature trend (red) and the second pair is for the cloud top pressure trend (green).

Figure 10 shows the time series and trends of the net shortwave, longwave, and all-wave radiative fluxes at the surface for four seasons and the annual mean for the Arctic region north of 60°N. The net radiative flux is defined as the downwelling minus upwelling fluxes. In winter, all of the net shortwave, longwave, and all-wave radiative fluxes exhibit negative trends due to the decreasing cloudiness in the central Arctic Ocean, but the trends are not statistically significant. There are positive trends in the net all-wave radiative flux at the surface at the annual rates of 0.42 W/m^2, 0.59 W/m^2, and 0.27 W/m^2 with the SDs of 0.22 W/m^2, 0.27 W/m^2, and 0.13 W/m^2 in spring, summer, and the annual mean, respectively. When the Sun is over the Arctic horizon, the net shortwave and longwave radiative fluxes tend to have opposite trends that are associated with the cloud forcing trends, that is, more clouds increase the net longwave radiative flux, but decrease the net shortwave radiative flux at the surface by reflecting more shortwave radiation back to the atmosphere.

Figure 11 shows the time series and trends in the shortwave, longwave, and all-wave cloud forcing for the entire Arctic region. In winter the net all-wave cloud forcing, which is dominated by the longwave cloud forcing with the trend of −0.17 W/m^2 per year, has decreased at the annual rate of −0.21 W/m^2 (decreasing warming effect) with an SD of 0.075 W/m^2 in response to a negative trend in cloud fraction (Figure 6). A strong cooling effect by clouds can be seen in the central Arctic Ocean. The decreasing trend in the shortwave cloud forcing at the annual rate of −0.04 W/m^2 only represents the sunlit part of the Arctic region for the latitudes lower than about 75°N. In the warm seasons, the increasing cloud fraction and warmer clouds in spring result in the increasing trend in the longwave cloud forcing (greater warming) at the annual rate of 0.102 W/m^2, but more clouds also result in a strong negative trend in the shortwave cloud forcing (greater cooling) at the annual rate of −0.325 W/m^2, such that there is a significant negative trend of −0.223 W/m^2 per year with an SD of 0.066 W/m^2 in the all-wave cloud forcing. While in summer, the shortwave cloud forcing is much larger in magnitude than in winter, and it dominates the net all-wave cloud forcing with the annual rate of −0.22 W/m^2. The longwave cloud forcing has been also decreasing at the annual rate of −0.045 W/m^2. Though the summer shortwave and longwave cloud forcing trends are not significant, the net all-wave cloud forcing resulting from the combination of the two is statistically significant and has the annual rate of −0.266 W/m^2 per year with an SD of 0.122 W/m^2. The strongest cooling effect exerted by cloud forcing occurred in the central Arctic Ocean and Arctic land areas. In autumn, the cloud cooling effect on the surface is less strong than that in winter and summer and statistically insignificant. Overall the annual mean trend in the all-wave cloud forcing is −0.211 W/m^2 per year with an SD of 0.053 W/m^2, indicating an increased cooling effect enforced by clouds on the surface.

The interactions between clouds, surface, and radiation field, that is, the cloud-surface-radiation feedback, are such that there are significant increasing trends in the net radiation budget in spring and summer. It appears that during the sunlit part of a year the decreases in sea ice extent and albedo that result from surface warming overtake the increasing cloud cooling effect, resulting in a net increasing trend in the surface all-wave radiation budget. However, the balance of these effects is influenced by other atmospheric factors as well, for example, air temperature and humidity. In general, the net shortwave radiative flux overwhelms the longwave radiative flux in the net all-wave radiative flux as shown in Figure 10. In the Chukchi Sea, for example, there are positive trends in the net shortwave and all-wave radiative fluxes in summer and autumn that is primarily due to the increasing trend in the surface temperature and a decreasing trend in surface albedo. With no trend in cloud fraction in this area, more shortwave radiation is absorbed by the surface in that area. Change in one surface property will not only affect other surface properties, but may also affect clouds as discussed in the paper by Liu et al. [22] which shows that decreasing sea ice concentration could result in increasing cloud cover locally to a certain degree. This implies that the cloud-radiation feedback may act to modulate the net surface radiative flux.

6. Sea Ice

Sea ice is probably the most important component of the Arctic climate system. It is also the unique and important indicator for the Arctic climate change in terms of sea ice extent, concentration, thickness, volume, and loss of multiyear ice. Combining APP-x data products with sea ice concentration data from microwave observations, the One-dimensional Thermodynamic Ice Model (OTIM) [34] was applied to estimate sea ice thickness and subsequently the sea ice volume for the Arctic Ocean north of 60°N. The OTIM was developed based on surface energy budget theory where the surface may be covered with snow. Validation of the model was performed with sea ice thickness measurements from submarine cruises, moorings, and stations. The overall uncertainty of the OTIM estimated ice thickness against ground truth is less than 20%. The model is described in detail in [34]. Figure 12 is an example of the OTIM retrieved sea ice thickness for the September of 2003.

The time series and trends of the total sea ice extent, concentration, thickness, and volume over 1982–2004 are shown in Figure 13 for September when Arctic sea ice extent and thickness are at their minimum for the year. The total ice extent within the Arctic has declined at the annual rate of −54,850 km^2 with an SD of 13,390 km^2. The area-average ice thickness has also decreased by 0.003 m per year, but it is not statistically significant. The total sea ice volume has declined at the annual rate of −56.12 km^3 with an SD of 18.82 km^3. The areal average sea ice concentration also shows a negative tendency at the annual rate of −0.13% with an SD of 0.087%.

Overall in the Arctic Ocean, sea ice extent, concentration, thickness, and volume have been all declining at the decadal rates of −8%, −1.4%, −5%, and −15%, respectively, consistent with a warming Arctic Ocean since 1982. Kwok and Rothrock [6] and Kwok and Untersteiner [7] found much larger decline rates in sea ice thickness and volume with the 10 Ice, Cloud, and Land Elevation Satellite (ICESat)

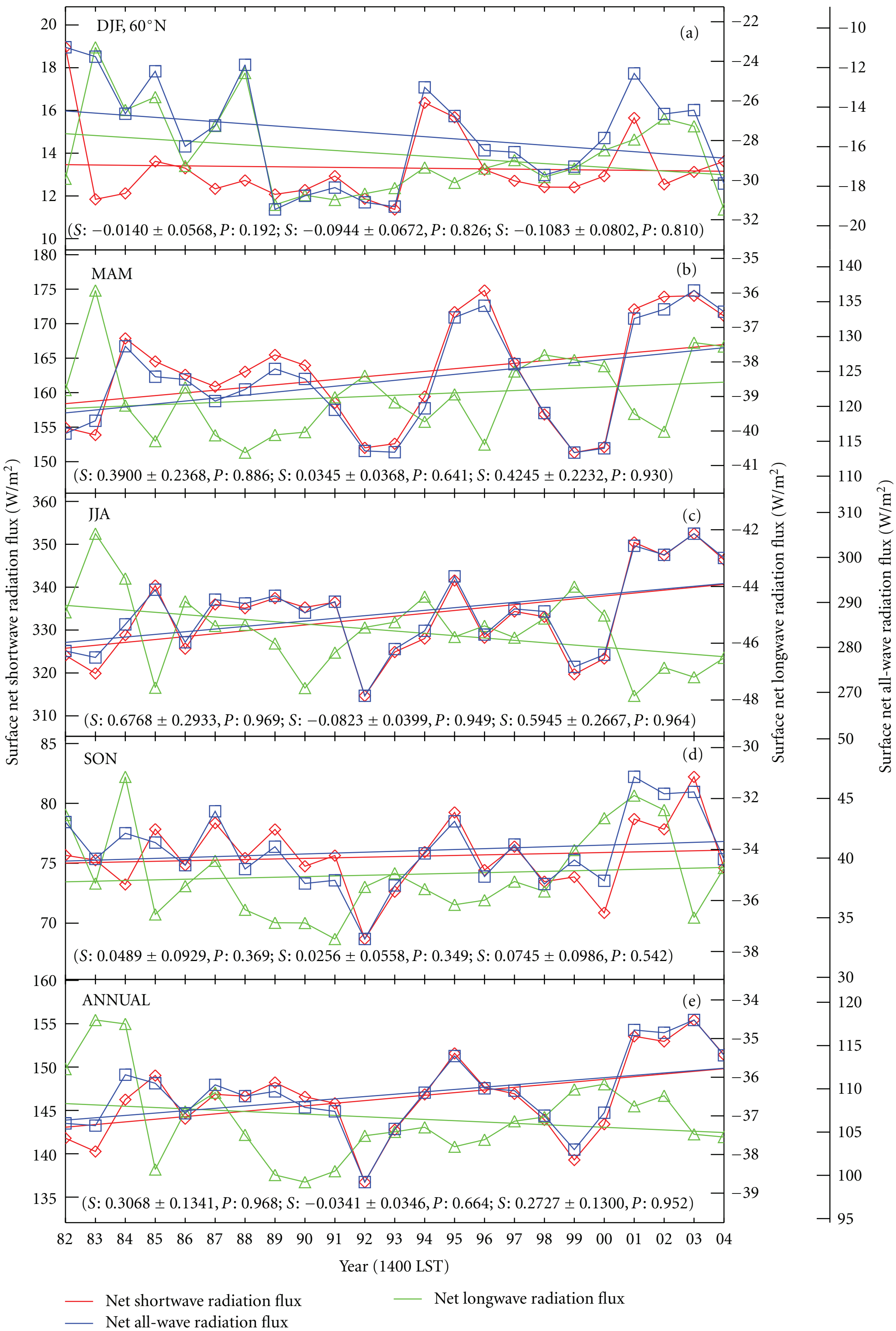

FIGURE 10: As in Figure 3, but for net shortwave, net longwave, and all-wave radiative fluxes at the surface. The first pair of S and P denotes the net shortwave radiation trend (red), the second pair is for the net longwave radiation trend (green), and the third pair represents the net all-wave radiation trend (blue).

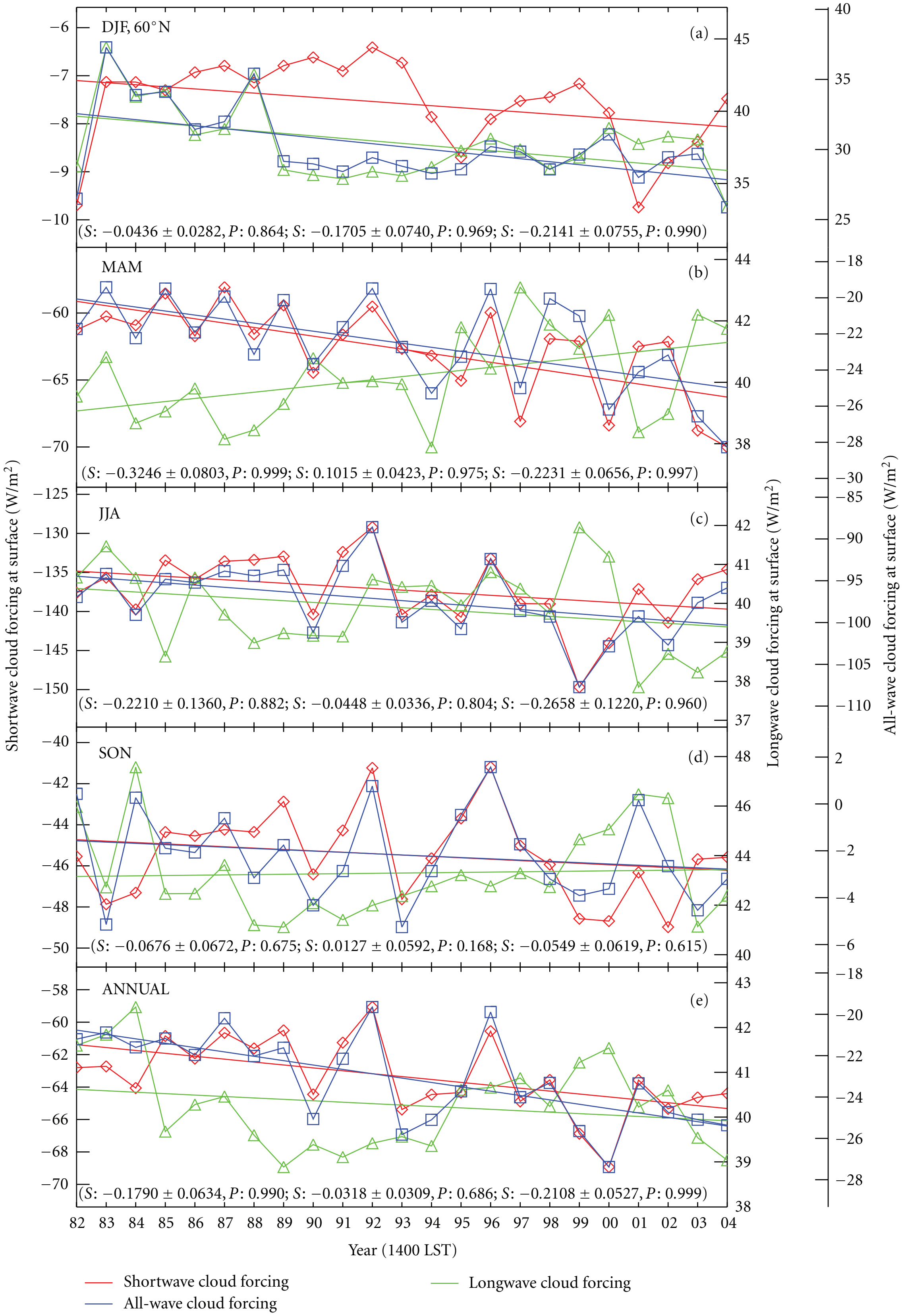

Figure 11: As in Figure 3, but for shortwave, longwave, and all-wave cloud forcing at the surface. The first pair of S and P denotes the shortwave cloud forcing trend (red), the second pair is for the longwave cloud forcing trend (green), and the third pair represents the all-wave cloud forcing trend (blue).

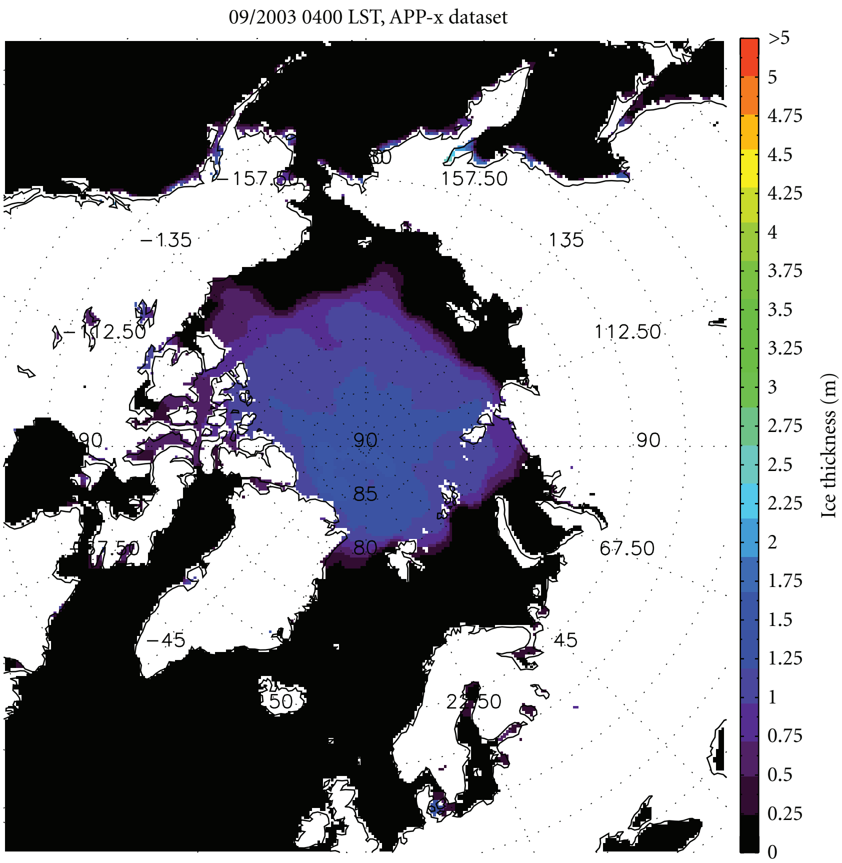

Figure 12: Spatial distribution of the monthly mean sea ice thickness for September 2003 retrieved by OTIM with APP-x data set for the Arctic Ocean north of 60°N.

campaigns that span a 5-year period between 2003 and 2008 that does not overlap with this study period and for the relatively smaller region covering the central Arctic Ocean only. In addition, from the microwave derived sea ice age and extent over 1982–2011, the loss of sea ice in the Arctic is totally from multiyear ice which is defined as sea ice survives at least one summer melt season. Figure 14 shows the time series and trends of total sea ice extent, first-year sea ice extent, multiyear sea ice extent, and the North Atlantic Oscillation (NAO) index over 1982–2011. The Arctic multiyear sea ice extent has declined at the annual rate of $-65{,}980\,km^2$ with an SD of $11{,}620\,km^2$, while in the meantime the first-year sea ice extent has oppositely increased at the annual rate of $15{,}960\,km^2$ with an SD of $11{,}580\,km^2$, but statistically insignificant. Consequently, the total sea ice extent has declined at the annual rate of $-51{,}330\,km^2$ with an SD of $5465\,km^2$.

7. Discussion

The analysis of the variations and trends in Arctic climate in the previous sections indicates the Arctic has indeed been warming up since 1980s, and this warming is accelerating starting from the end of 20th century. The warming is in concert with a global warming, though the Arctic is warming at a greater rate, a phenomenon called "Arctic Amplification" (AA) [53]. A recent study by Francis and Vavrus shows that Arctic amplification may cause more persistent weather patterns in midlatitudes that can lead to extreme weather [54]. The scope of the trends identified here also suggests that the interactions between the Arctic and lower-latitude regions are likely to play important roles in Arctic climate change.

Corresponding to the Arctic sea ice decline over 1982–2011, the North Atlantic Oscillation (NAO) has also shown a significant negative trend at the annual rate of −0.022 with an SD of 0.007 towards the more negative phase (Figure 14). Other climate indices can also be used to better understand the relationship between Arctic climate change and global climate change. The most commonly used climate indices include the Arctic Oscillation (AO), the NAO, the Antarctic Oscillation (AAO), the Southern Oscillation (SO), the Multivariate ENSO Index (MEI), the Pacific Decadal Oscillation (PDO), the Pacific-North American (PNA) Pattern, and the Madden-Julian oscillation (MJO). Figure 15 shows the variability of the climate indices since 1950. It appears that there are significant turning points in most of the climate indices that occurred in the late 1970s and early 1980s when the global climate has been warming up, as stated in IPCC Fourth Assessment Report [55]. Correspondingly, Arctic climate has been also changing rapidly with profound impacts on environmental, ecological,

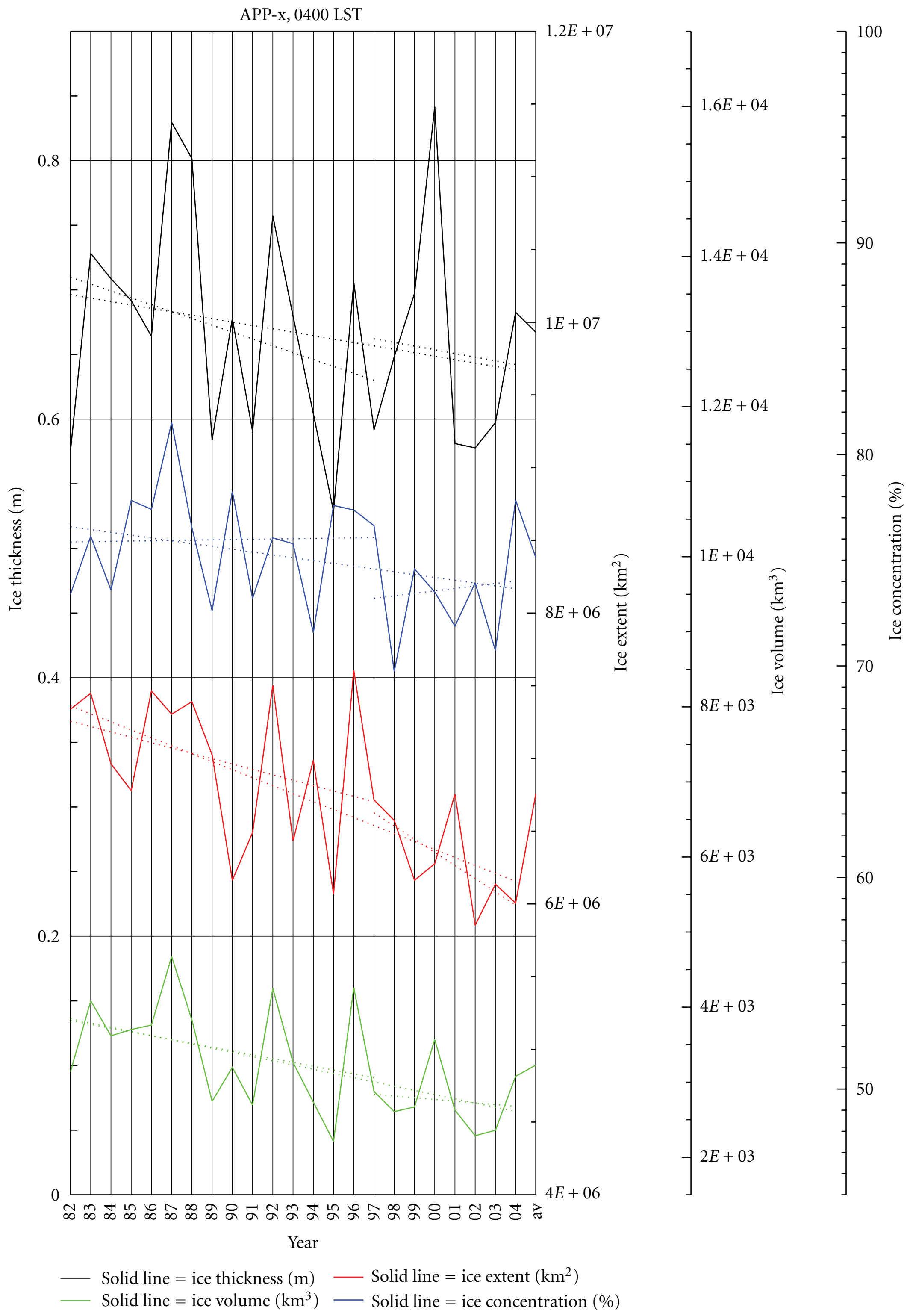

FIGURE 13: Time series of monthly mean sea ice extent, concentration, thickness, and volume for September over the period 1982–2004 for the Arctic Ocean north of 60°N.

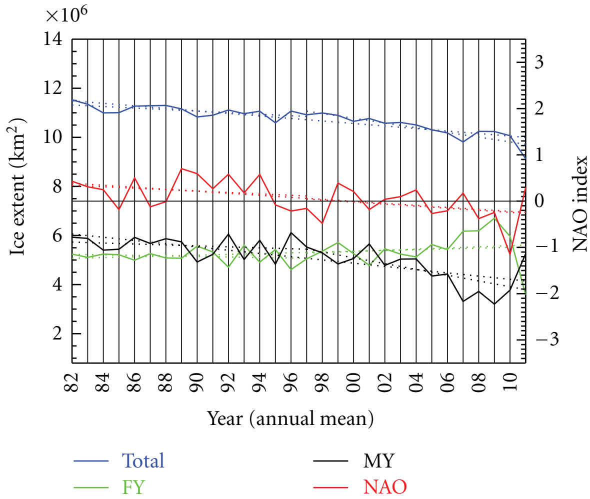

Figure 14: Time series of Arctic first-year sea ice extent, multiyear sea ice extent, and total (first-year plus multiyear) sea ice extent, and NAO index over the period 1982–2011 for the Arctic region north of 60°N.

and biological cycles. Is there any link between Arctic climate change and global climate change? What areas in the Arctic are most sensitive to global climate change? To answer those questions, correlation coefficients between climate indices and surface skin temperature anomalies (SSTAs) were calculated for each pixel in the Arctic for winter, spring, summer, autumn, and the annual mean based on the 23-year monthly data. The student's t-test was used to examine at what confidence level a correlation coefficient is statistically significant.

Figure 16 is the correlation coefficient image between AO indices and surface temperature anomalies from 276 months during the period of 1982 to 2004. The contours in the image represent confidence levels. It clearly shows that different areas in the Arctic have different correlations with AO. Though the warming is prevalent in the Arctic in all seasons except winter over the central Arctic Ocean, the relationships of the AO and the surface temperature anomalies are quite different in different areas. For example, there is a positive correlation in the eastern part of the Arctic, but a negative correlation in the western part of the Arctic. Northern Europe and northern Russia have positive correlations with the AO, while Greenland and northern Canada have negative correlations in all seasons except for a weak positive correlation in northern Canada in summer. The highest correlation occurs in winter, and the weakest correlation is in summer, as expected given the nature of the AO. The AO can explain about 30% of the variation in surface temperature in North Europe, Baffin Bay, and Greenland in winter, and on an annual time scale it explains about 25% of the variance in surface temperature. The correlation between NAO and SSTA is very similar to that between AO and SSTA; the other climate indices show much weaker correlations with SSTA than AO and NAO as shown in [15].

The analysis of the relationships between Arctic surface skin temperature anomalies and climate indices suggests that the global climate interacts with the Arctic climate to a certain degree. Arctic climate change is, indeed, closely related to global large-scale circulation changes in both the atmosphere and ocean. Changes in the global climate seen in the AO and the NAO can explain at least 25% of the changes in Arctic climate in every season in some areas, for example, Greenland. Table 3 lists the correlation coefficients between surface temperature anomalies and the AO and NAO indices using both the original time series and the detrended time series. Each of the detrended time series was obtained by removing its linear trend, that is, the slope of the linear regression line, from its original time series. The two sets of correlation coefficients are nearly identical in value and confidence. It is clear that there are some areas in the Arctic that are more sensitive to global climate change than other areas. Those areas should be very useful in monitoring and predicting Arctic climate change caused by, at least in part, changes outside of the Arctic.

8. Conclusions

Satellite data provide a unique and unprecedented opportunity to gain knowledge of environment, weather, and climate in the remote and data-sparse areas like the Arctic and Antarctic. The APP-x data set provides climate data records of surface, cloud, radiation, and cryosphere properties for the Arctic. This study investigated recent Arctic climate variabilities and trends based on the updated APP-x data set. As shown in the previous sections, the Arctic as a whole appears to be warming rapidly at the surface, but the sign and magnitude of the changes vary in time and location. On an annual time scale the entire Arctic has been warming, but cooling has also been observed over much of the Arctic Ocean in winter, except for the Beaufort Sea, Baffin Bay, Canada Archipelago Seas, Hudson Bay, and Canada Basin, where the trends are not statistically significant. The strongest cooling occurred in the eastern central Arctic Ocean at

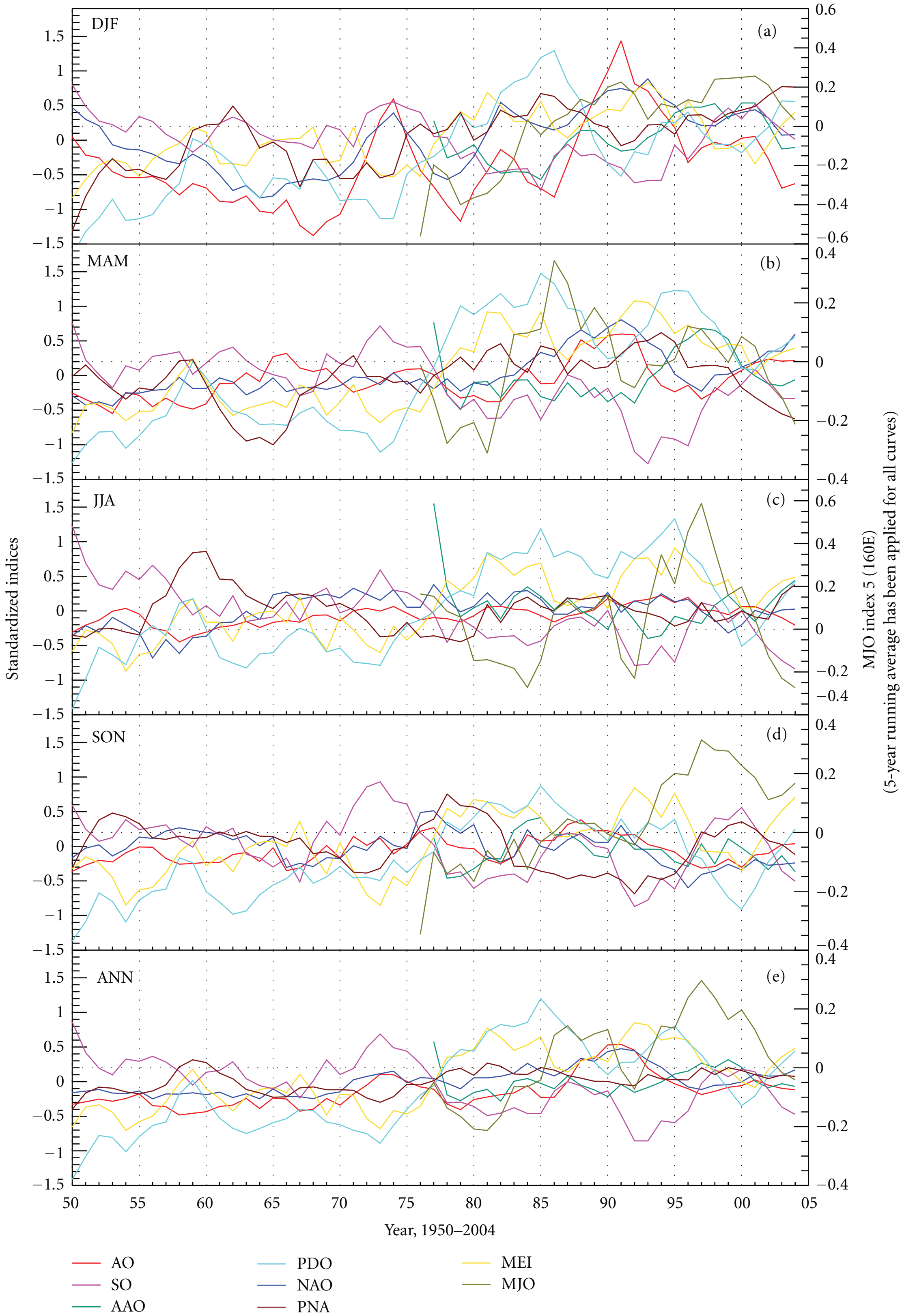

Figure 15: Time series of the eight commonly used climate indices in winter (DJF), spring (MAM), summer (JJA), autumn (SON) and the annual mean over the period 1950–2004.

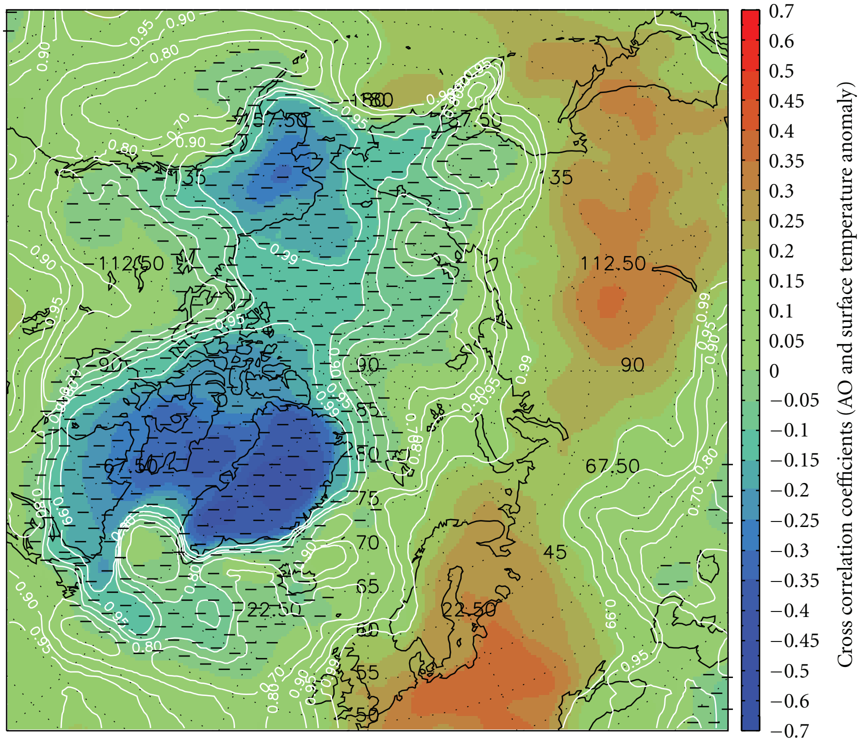

FIGURE 16: Correlation between the AO index and surface temperature anomalies from 276 months during the period 1982–2004. Contours in the image are confidence levels.

TABLE 3: Correlation between surface skin temperature anomalies and AO/NAO indices for the 18 Arctic sub-regions based on 276 months.

Area name and ID no.*	AO		NAO	
	Original	Detrended	Original	Detrended
Beaufort sea (1)	**−0.1905 (99%)**	**−0.1850 (99%)**	**−0.1832 (99%)**	**−0.1662 (99%)**
Chukchi sea (2)	**−0.1696 (99%)**	**−0.1647 (99%)**	−0.1380 (88%)	−0.0594 (84%)
Canada basin (3)	**−0.1717 (99%)**	**−0.1681 (99%)**	−0.0809 (91%)	−0.0718 (88%)
Central arctic (4)	**−0.1067 (96%)**	**−0.1061 (96%)**	−0.0128 (58%)	−0.0113 (57%)
Laptev sea (5)	−0.0278 (68%)	−0.0327 (71%)	0.0813 (91%)	0.0718 (88%)
North pole (6)	−0.0508 (80%)	−0.0564 (82%)	0.0795 (91%)	0.0690 (87%)
Nansen basin (7)	−0.0123 (58%)	−0.0134 (59%)	**0.1471 (99%)**	**0.1454 (99%)**
Kara and Barents sea (8)	**0.1923 (99%)**	**0.1874 (99%)**	**0.2561 (99%)**	**0.2441 (99%)**
GIN seas (9)	0.0316 (70%)	0.0304 (69%)	0.0531 (81%)	0.0508 (80%)
Baffin bay (10)	**−0.3594 (99%)**	**−0.3623 (99%)**	**−0.3147 (99%)**	**−0.2996 (99%)**
Canada archipelago seas (11)	**−0.2675 (99%)**	**−0.2637 (99%)**	**−0.2513 (99%)**	**−0.2378 (99%)**
Hudson bay (12)	**−0.3190 (99%)**	**−0.3207 (99%)**	**−0.3327 (99%)**	**−0.3186 (99%)**
North Europe (13)	**0.3661 (99%)**	**0.3798 (99%)**	**0.2705 (99%)**	**0.2933 (99%)**
North central Russia (14)	**0.3051 (99%)**	**0.3063 (99%)**	**0.1454 (99%)**	**0.1480 (99%)**
Northeastern Russia (15)	0.0478 (79%)	0.0530 (81%)	−0.0401 (75%)	−0.0299 (70%)
Alaska region (16)	**−0.2370 (99%)**	**−0.2328 (99%)**	**−0.1493 (92%)**	**−0.1298 (99%)**
North Canada (17)	**−0.1875 (99%)**	**−0.1829 (99%)**	**−0.2958 (99%)**	**−0.2794 (99%)**
Greenland Island (18)	**−0.4157 (99%)**	**−0.4164 (99%)**	**−0.4534 (99%)**	**−0.4443 (99%)**

*Numbers in parenthesis in the second and third columns are the student's t-test confidence level for the above correlation coefficient. Bold type indicates correlations with confidence levels of 95% or higher. Correlations were done with original time series (Original) and detrended time series (Detrended) as marked in the first table row.

the annual rate of -0.20°C in winter. In the warm seasons (spring, summer, and autumn), all significant trends in surface skin temperature are positive. The strongest warming is over northern Canada where the annual rates of the surface temperature changes are 0.10°C, 0.07°C, 0.15°C, 0.17°C, and 0.11°C for winter, spring, summer, autumn, and the annual mean, respectively.

Arctic cloud properties have been changing, especially in winter and in spring when negative and positive cloud fraction trends were found. Clouds have become more liquid phase, likely with smaller cloud particle effective radius and higher cloud top height over the warmer surface areas. Cloud optical depth does not show significant trends except over the northern Canada, where significant positive trends were found in summer and autumn, and over the GIN Seas where negative trends were found all the year round. In addition, cloud height increased significantly in warm seasons over most of the Arctic areas. The net all-wave radiative flux at the surface shows a significant negative trend in winter over most of the Arctic Ocean areas due to the negative trends in cloud fraction; positive trends have been found in warm seasons over most of the Arctic landmasses and ocean areas. The interactions between clouds, surface, radiation, and atmospheric conditions, commonly called the cloud-surface-radiation feedback, work together to cause significant negative trends in the net radiative flux in winter and positive trends during warm seasons for most of the Arctic areas. However, the trends in cloud forcing are always negative for all seasons, indicating a damping effect on the surface warming by clouds. It appears that during the sunlit part of a year the negative trends in sea ice extent and surface albedo from surface warming modulate the cloud damping effect on the surface warming to some degree, which results in positive trends in the net surface radiative flux during warming seasons.

Arctic sea ice is a unique and critical parameter of the Arctic climate system. Changes in sea ice can reflect and impact Arctic climate state to a much larger extent than in any other regions. It is obvious from this study that Arctic sea ice has been declining significantly since the 1980s, with the overall decadal rates of -8%, -1.4%, -5%, and -15% in sea ice extent, concentration, thickness, and volume, respectively. These changes indicate that Arctic warming has casused substantial changes to the cryosphere, which may lead Arctic climate towards to another unprecedented equilibratory state. Some studies [6, 7] reported even more rapid declines in sea ice volume, as high as -40% per decade from 2003 to 2008.

All the commonly used climate indices imply a significant turning point of the global climate in the late 1970s and early 1980s along with an accelerated Arctic warming. The correlation analysis of the AO/NAO and surface skin temperature anomalies, cloud fraction anomalies, and precipitable water anomalies in the Arctic indicates that there is at least a statistical linkage between Arctic climate change and global climate change for some sensitive Arctic areas. Feedback mechanisms should be investigated further using both models and observations, and additional research is needed in order to determine to what degree Arctic climate change is due to local processes (e.g., evaporation) and large-scale circulation.

Most previous studies of Arctic climate that were based on satellite data focused on a specific climate parameter. Our study assesses trends in many of the major Arctic climate parameters. Agarwal et al. (2011) [56] used Advanced Very-High-Resolution Radiometer (AVHRR) Polar Pathfinder (APP) data over a 23-year period to study the decadal to seasonal variability of the clear-sky Arctic sea ice albedo. Comiso (2003) [57] used AVHRR data to examine the clear-sky Arctic surface temperature trend over the period 1981–2001; his results are very similar to ours in terms of season and value, for example, cooling trend found in winter for central Arctic ocean both in his study and ours. Schweiger (2004) [58] compared cloud trends from the TOVS (TIROS Operational Vertical Sounder) Polar Pathfinder retrievals and two AVHRR datasets, including an earlier version of APP-x, and found similar trends over the period 1980–2001. Regarding the trends in sea ice, Kwok and Rothrock [6] and Kwok and Untersteiner [7] (2009) found much larger autumn rates of decline: 20 cm per year and 1237 km^3 per year in sea ice thickness and volume, respectively, but for the 5-year period between 2003 and 2008 when Arctic sea ice changes were significant and for the relatively smaller region covering the central Arctic Ocean. Maslanik et al. (2007) [37] used a different technique to estimate sea ice thickness from sea ice age with microwave data for the period of 1982–2006, but did not examine trends. Similarities and differences between these studies warrant further investigation.

Acknowledgments

This work was supported by the National Science Foundation Grant ARC-1023371, NOAA Climate Data Records Program, NASA ROSES Science of Terra and Aqua Program, and NASA NPP Science Team for Climate Data Records Program. The National Snow and Ice Data Center (NSIDC) provided the standard APP data and sea ice concentration data. The NCEP/NCAR reanalysis global profile data set was provided by NOAA-CIRES Climate Diagnostics Center. NASA Langley Research Center provided the ISCCP D2 ozone data set. The views, opinions, and findings contained in this paper are those of the author(s) and should not be construed as an official National Oceanic and Atmospheric Administration or US Government position, policy, or decision.

References

[1] D. A. Rothrock, Y. Yu, and G. A. Maykut, "Thinning of the Arctic Sea-Ice cover," *Geophysical Research Letters*, vol. 26, no. 23, pp. 3469–3472, 1999.

[2] K. Y. Vinnikov, A. Robock, R. J. Stouffer et al., "Global warming and Northern Hemisphere sea ice extent," *Science*, vol. 286, no. 5446, pp. 1934–1937, 1999.

[3] C. L. Parkinson, D. J. Cavalieri, P. Gloersen, H. J. Zwally, and J. C. Comiso, "Arctic sea ice extents, areas, and trends, 1978–1996," *Journal of Geophysical Research C*, vol. 104, no. 9, pp. 20837–20856, 1999.

[4] D. J. Cavalieri, C. L. Parkinson, and K. Y. Vinnikov, "30-year satellite record reveals contrasting Arctic and Antarctic

decadal sea ice variability," *Geophysical Research Letters*, vol. 30, no. 18, p. 4, 2003.

[5] J. A. Maslanik, C. Fowler, J. Stroeve et al., "A younger, thinner Arctic ice cover: increased potential for rapid, extensive sea-ice loss," *Geophysical Research Letters*, vol. 34, no. 24, Article ID L24501, 2007.

[6] R. Kwok and D. A. Rothrock, "Decline in Arctic sea ice thickness from Decline in Arctic sea ice thickness from submarine and ICESat records: 1958–2008," *Geophysical Research Letters*, vol. 36, Article ID L15501, 5 pages, 2009.

[7] R. Kwok and N. Untersteiner, "The thinning of Arctic sea ice," *Physics Today*, vol. 64, no. 4, pp. 36–41, 2011.

[8] J. C. Comiso, "Large decadal decline of the arctic multiyear ice cover," *Journal of Climate*, vol. 25, no. 4, pp. 1176–1193, 2012.

[9] J. A. Curry, W. B. Rossow, D. Randall, and J. L. Schramm, "Overview of arctic cloud and radiation characteristics," *Journal of Climate*, vol. 9, no. 8, pp. 1731–1764, 1996.

[10] I. G. Rigor, R. L. Colony, and S. Martin, "Variations in surface air temperature observations in the Arctic, 1979–97," *Journal of Climate*, vol. 13, no. 5, pp. 896–914, 2000.

[11] Y. Chen, J. A. Francis, and J. R. Miller, "Surface temperature of the Arctic: comparison of TOVS satellite retrievals with surface observations," *Journal of Climate*, vol. 15, no. 24, pp. 3698–3708, 2002.

[12] D. G. Groves and J. A. Francis, "Variability of the Arctic atmospheric moisture budget from TOVS satellite data," *Journal of Geophysical Research*, vol. 107, no. 24, pp. 4785–4800, 2002.

[13] X. Wang and J. R. Key, "Recent trends in arctic surface, cloud, and radiation properties from space," *Science*, vol. 299, no. 5613, pp. 1725–1728, 2003.

[14] X. Wang and J. R. Key, "Arctic surface, cloud, and radiation properties based on the AVHRR polar pathfinder dataset. Part I: spatial and temporal characteristics," *Journal of Climate*, vol. 18, no. 14, pp. 2558–2574, 2005.

[15] X. Wang and J. R. Key, "Arctic surface, cloud, and radiation properties based on the AVHRR polar pathfinder dataset. Part II: recent trends," *Journal of Climate*, vol. 18, no. 14, pp. 2575–2593, 2005.

[16] J. A. Francis, D. M. White, J. J. Cassano et al., "An arctic hydrologic system in transition: feedbacks and impacts on terrestrial, marine, and human life," *Journal of Geophysical Research*, vol. 114, Article ID G04019, 2009.

[17] D. W. J. Thompson and J. M. Wallace, "The Arctic oscillation signature in the wintertime geopotential height and temperature fields," *Geophysical Research Letters*, vol. 25, no. 9, pp. 1297–1300, 1998.

[18] J. M. Wallace and D. S. Gutzler, "Teleconnections in the geopotential height field during the Northern Hemisphere winter," *Monthly Weather Review*, vol. 109, no. 4, pp. 784–812, 1981.

[19] N. J. Mantua, S. R. Hare, Y. Zhang, J. M. Wallace, and R. C. Francis, "A pacific interdecadal climate oscillation with impacts on salmon production," *Bulletin of the American Meteorological Society*, vol. 78, no. 6, pp. 1069–1079, 1997.

[20] Y. Zhang, J. M. Wallace, and D. S. Battisti, "ENSO-like interdecadal variability: 1900–93," *Journal of Climate*, vol. 10, no. 5, pp. 1004–1020, 1997.

[21] J. C. Stroeve, J. Maslanik, M. C. Serreze, I. Rigor, W. Meier, and C. Fowler, "Sea ice response to an extreme negative phase of the Arctic Oscillation during winter 2009/2010," *Geophysical Research Letters*, vol. 38, no. 2, Article ID L02502, 2011.

[22] Y. Liu, J. R. Key, Z. Liu, X. Wang, and S. J. Vavrus, "A cloudier Arctic expected with diminishing sea ice," *Geophysical Research Letters*, vol. 39, Article ID L05705, 2012.

[23] S. Manabe and R. J. Stouffer, "Multiple-century response of a coupled ocean-atmosphere model to an increase of atmospheric carbon dioxide," *Journal of Climate*, vol. 7, no. 1, pp. 5–23, 1994.

[24] S. Manabe, M. J. Spelman, and R. J. Stouffer, "Transient response of a coupled ocean-atmosphere model to gradual changes of atmospheric CO_2. Part II: seasonal response," *Journal of Climate*, vol. 5, no. 2, pp. 105–126, 1992.

[25] G. A. Meehl and W. M. Washington, "CO_2 climate sensitivity and snow-sea-ice albedo parameterization in an atmospheric GCM coupled to a mixed-layer ocean model," *Climatic Change*, vol. 16, no. 3, pp. 283–306, 1990.

[26] J. R. Miller and G. L. Russell, "Projected impact of climate change on the freshwater and salt budgets of the Arctic Ocean by a global climate model," *Geophysical Research Letters*, vol. 27, no. 8, pp. 1183–1186, 2000.

[27] J. A. Francis and S. J. Vavrus, "Evidence linking arctic amplification to extreme weather in Mid-Latitudes," *Geophysical Research Letters*, vol. 39, Article ID L06801, 2012.

[28] C. Fowler, J. Maslanik, T. Haran, T. Scambos, J. Key, and W. Emery, *AVHRR Polar Pathfinder Twice-Daily 25 km EASE-Grid Composites*, National Snow and Ice Data Center, Digital Media, Boulder, Colo, USA, 2002.

[29] J. R. Key and A. J. Schweiger, "Tools for atmospheric radiative transfer: STREAMER and FLUXNET," *Computers and Geosciences*, vol. 24, no. 5, pp. 443–451, 1998.

[30] J. Key and A. J. Schweiger, *FluxNet User's Guide*, NOAA/NESDIS/ORA/ARAD/ ASPT, University of Wisconsin, Dayton, Ohio, USA, 2000.

[31] J. Key, *The Cloud and Surface Parameter Retrieval (CASPR) System for Polar AVHRR User's Guide*, NOAA/NESDIS/ORA/ASPT, University of Wisconsin, Dayton, Ohio, USA, 2002.

[32] J. R. Key, X. Wang, J. C. Stoeve, and C. Fowler, "Estimating the cloudy-sky albedo of sea ice and snow from space," *Journal of Geophysical Research D*, vol. 106, no. 12, pp. 12489–12497, 2001.

[33] J. R. Key, P. Yang, A. Bryan Baum, and S. L. Nasin, "Parameterization of shortwave ice cloud optical properties for various particle habits," *Journal of Geophysical Research*, vol. 107, no. 13, p. 4181, 2002.

[34] X. Wang, J. R. Key, and Y. Liu, "A thermodynamic model for estimating sea and lake ice thickness with optical satellite data," *Journal of Geophysical Research*, vol. 115, no. 12, pp. 1–14, 2011.

[35] W. B. Rossow and E. N. Dueñas, "The International Satellite Cloud Climatology Project (ISCCP) web site: an online resource for research," *Bulletin of the American Meteorological Society*, vol. 85, no. 2, pp. 167–172, 2004.

[36] J. R. Key and J. M. Intrieri, "Cloud particle phase determination with the AVHRR," *Journal of Applied Meteorology*, vol. 39, no. 10, pp. 1797–1804, 2000.

[37] J. A. Maslanik, J. Key, C. W. Fowler, T. Nguyen, and X. Wang, "Spatial and temporal variability of satellite-derived cloud and surface characteristics during FIRE-ACE," *Journal of Geophysical Research D*, vol. 106, no. 14, pp. 15233–15249, 2001.

[38] J. C. Stroeve, J. E. Box, C. Fowler, T. Haran, and J. Key, "Intercomparison between in situ and AVHRR polar pathfinder-derived surface albedo over Greenland," *Remote Sensing of Environment*, vol. 75, no. 3, pp. 360–374, 2001.

[39] M. Pavolonis and J. Key, "Antarctic cloud radiative forcing at the surface estimated from the AVHRR Polar Pathfinder and ISCCP D1 data sets, 1985–1993," *Journal of Applied Meteorology*, vol. 42, no. 6, pp. 827–840, 2003.

[40] M. C. Serreze, J. E. Walsh, F. S. Chapin et al., "Observational evidence of recent change in the northern high-latitude environment," *Climatic Change*, vol. 46, no. 1-2, pp. 159–207, 2000.

[41] J. C. Comiso, D. J. Cavalieri, C. L. Parkinson, and P. Gloersen, "Passive microwave algorithms for sea ice concentration: a comparison of two techniques," *Remote Sensing of Environment*, vol. 60, no. 3, pp. 357–384, 1997.

[42] D. R. Thomas and D. A. Rothrock, "The arctic ocean ice balance: a kalman smoother estimate," *Journal of Geophysical Research*, vol. 98, no. 6, pp. 10053–10067, 1993.

[43] D. G. Groves and J. A. Francis, "Moisture budget of the Arctic from TOVS satellite data," *Journal of Geophysical Research*, vol. 107, no. 19, p. 4391, 2002.

[44] M. C. Serreze and R. G. Barry, "Atmospheric components of the Arctic Ocean hydrologic budget assessed from rawinsonde data," in *The Fresh-water Budget of the Arctic Ocean*, E. L. Lewis, Ed., pp. 141–161, Kluwer Academic, Norwell, Mass, USA, 2000.

[45] J. E. Overland, M. Wang, and N. A. Bond, "Recent temperature changes in the western Arctic during spring," *Journal of Climate*, vol. 15, no. 13, pp. 1702–1716, 2002.

[46] O. M. Johannessen, E. V. Shalina, and M. W. Miles, "Satellite evidence for an Arctic sea ice cover in transformation," *Science*, vol. 286, no. 5446, pp. 1937–1939, 1999.

[47] K. Y. Vinnikov, A. Robock, R. J. Stouffer et al., "Global warming and Northern Hemisphere sea ice extent," *Science*, vol. 286, no. 5446, pp. 1934–1937, 1999.

[48] E. Rignot and R. H. Thomas, "Mass balance of polar ice sheets," *Science*, vol. 297, no. 5586, pp. 1502–1506, 2002.

[49] M. R. Anderson and S. D. Drobot, "Spatial and temporal variability in snowmelt onset over Arctic sea ice," *Annals of Glaciology*, vol. 33, no. 1, pp. 74–78, 2001.

[50] D. J. Cavalieri, C. L. Parkinson, and K. Y. Vinnikov, "30-year satellite reveals contrasting Arctic and Antarctic decadal sea ice variability," *Geophysical Research Letters*, vol. 30, no. 18, p. 1970, 2003.

[51] Y. Liu, J. R. Key, and X. Wang, "Influence of changes in sea ice concentration and cloud cover on recent Arctic surface temperature trends," *Geophysical Research Letters*, vol. 36, Article ID L20710, 2009.

[52] Y. Liu, J. R. Key, J. A. Francis, and X. Wang, "Possible causes of decreasing cloud cover in the Arctic winter, 1982–2000," *Geophysical Research Letters*, vol. 34, Article ID L14705, 2007.

[53] M. C. Serreze and R. G. Barry, "Processes and impacts of Arctic amplification: a research synthesis," *Global and Planetary Change*, vol. 77, no. 1-2, pp. 85–96, 2011.

[54] J. A. Francis and S. J. Vavrus, "Evidence linking Arctic amplification to extreme weather in mid-latitudes," *Geophysical Research Letters*, vol. 39, Article ID L06801, 2012.

[55] S. Solomon, D. Qin, M. Manning et al., *Contribution of Working Group I to the Fourth Assessment Report of the Intergovernmental Panel on Climate Change*, Cambridge University Press, Cambridge, UK, 2007.

[56] S. Agarwal, W. Moon, and J. S. Wettlaufer, "Decadal to seasonal variability of Arctic sea ice albedo," *Geophysical Research Letters*, vol. 38, Article ID L20504, 2011.

[57] J. C. Comiso, "Warming trends in the Arctic from clear sky satellite observations," *Journal of Climate*, vol. 16, no. 21, pp. 3498–3510, 2003.

[58] A. J. Schweiger, "Changes in seasonal cloud cover over the Arctic seas from satellite and surface observations," *Geophysical Research Letters*, vol. 31, Article ID L12207, 4 pages, 2004.